Current direction dependent spin Hall magnetoresistance in epitaxial Pt/Co bilayers on MgO(110)

Ryan Thompson [1], Jeongchun Ryu,[2] Ye Du [1,3] Shutaro Karube,[1,4] Makoto Kohda,[1,3,4] and Junsaku Nitta[1,3,4,*]

[1]*Department of Materials Science, Graduate School of Engineering, Tohoku University, Sendai 980-8579, Japan*
[2]*Department of Materials Science and Engineering, KAIST, Daejeon 34141, South Korea*
[3]*Center for Science and Innovation in Spintronics (Core Research Cluster) Organization for Advanced Studies,*
Tohoku University, Sendai 980-8577, Japan
[4]*Center for Spintronics Research Network, Tohoku University, Sendai 980-8577, Japan*

We demonstrate that the spin Hall magnetoresistance (SMR) of epitaxial Pt/Co bilayers on MgO(110) single crystal substrates is strongly anisotropic and depends on the applied current direction with respect to the two primary in-plane crystal directions [001] and [$1\bar{1}0$], in the Pt layer. SMR results at different temperatures qualitatively suggest the D'yakonov-Perel spin relaxation mechanism through the invariance of the spin diffusion length λ_{sf} for a given current direction, while also suggesting an anisotropic Rashba-Edelstein effect from the ratio of $\lambda_{sf}^{[001]}$ to $\lambda_{sf}^{[1\bar{1}0]}$. Finally, deviation from the standard SMR model spurs the need for new theory that properly characterizes and quantifies the anisotropies in such epitaxial systems.

I. INTRODUCTION

Heavy metal/ferromagnetic (HM/FM) heterostructures have been extensively studied in recent years [1] due to the large spin-orbit coupling that allows for efficient charge current to spin current conversion (characterized by the spin Hall angle θ_{SH}) via the spin Hall effect (SHE) [2]. While studies have primarily used polycrystalline or amorphous systems, recent studies have shown significant contributions to the spin-orbit torque of epitaxial Pt/Co [3] by the Rashba-Edelstein (RE) effect [4–6], enhanced spin current generation in epitaxial Ta/CoFeB due to the extrinsic contribution to θ_{SH} [7], and highly efficient spin-orbit torque induced magnetization switching in epitaxial Au/Fe$_4$N [8].

The Rashba effect arises due to the broken inversion symmetry of an interface which creates an effective electric field at that interface which moving electrons feel as an effective magnetic field [9], and has been observed in metallic/ferromagnetic heterostructures [10,11], shown to induce spin torque in a ferromagnetic metal layer [12], and has even been predicted to be used as a method for electric field control of magnetism [13].

Pt is normally dominated by the Elliott-Yafet (EY) spin relaxation mechanism [14], in which momentum scattering events (for example due to phonons or impurities) cause spin to relax due to the coupling of spin and momentum [15,16], as is commonly the case in metals [17–20]. However, it has been shown that in the case of single crystal Pt where scattering events are suppressed, the D'yakonov-Perel (DP) mechanism [21] can instead be dominant [22]. The DP mechanism is caused by spin precession around an effective magnetic field, such as the Rashba field caused by the RE effect, and is distinct from the EY mechanism in that scattering events instead suppress spin relaxation.

In this paper we experimentally demonstrate strongly anisotropic spin Hall magnetoresistance (SMR) in epitaxial Pt/Co heterostructures grown on MgO(110), the magnitude and behavior of which greatly depends on the direction of the applied charge current. Our fitting results qualitatively suggest this is due to anisotropy in the spin diffusion length, caused by a combination of an anisotropic Fermi surface and a current-direction dependent RE effect. However, due to deviations from the standard SMR model, the obtained quantitative data must be considered carefully, spurring the need for further research and understanding in such epitaxial HM/FM systems.

II. FABRICATION AND CHARACTERIZATION

Pt(t_N nm)/Co(t_F nm)/AlO$_x$(2 nm) heterostructures were deposited on single crystal MgO(110)-oriented substrates using RF magnetron sputtering. In order to create good epitaxy, Pt was sputtered at 200°C. The sample was allowed to cool to room temperature in the vacuum chamber before sputtering the Co and AlO$_x$ layers in order to limit diffusion between the Pt and Co layers, and to keep the interface flat. The Co grows epitaxially on the fcc Pt in the hcp phase, as indicated by RHEED and in-plane XRD phi scan measurements seen in Figs. 1(b) and 1(c), respectively. RHEED shows a clear streak pattern even after 20 nm deposition of both Pt and Co layers, while the phi scan shows the expected twofold symmetry for both the (002) and (220) peaks of Pt and the (0001) and ($11\bar{2}0$) peaks of Co, with no other extraneous peaks, confirming an epitaxial crystal structure for both layers.

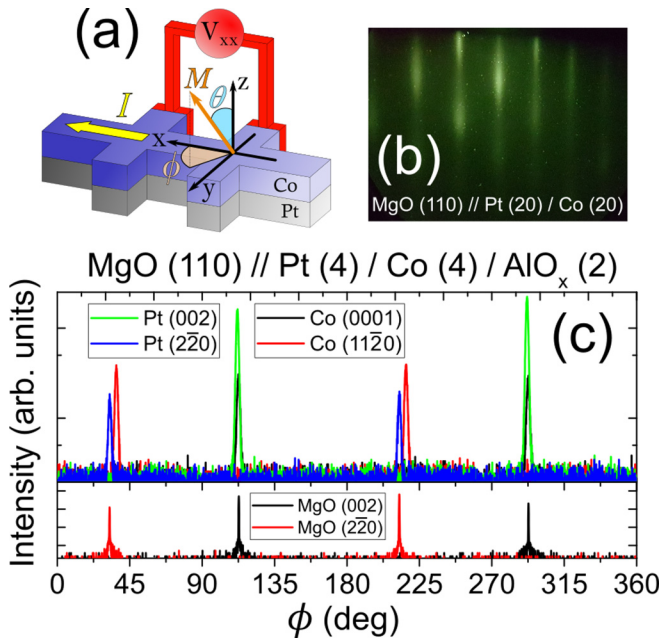*Corresponding author: nitta@material.tohoku.ac.jp

FIG. 1. (a) Hall bar geometry and definition of axes and angles. For all Hall bar orientations, $\hat{x}$ is the applied current direction, $\hat{z}$ is the out-of-plane direction, θ is the angle from the z axis, and ϕ is the angle from the x axis. (b) RHEED pattern of Pt(20)/Co(20) sample showing clear streak pattern. (c) In-plane XRD ϕ scan for Pt and Co layers showing clear twofold symmetry for both (002) and (220) peaks of Pt and (0001) and (11$\bar{2}$0) peaks of Co, confirming epitaxial crystal structure. The bottom phi scan shows the MgO substrate (002) and (220) peaks.

Co grows with its c axis growing in-plane along the Pt [001] direction, which is the reason for the strong uniaxial in-plane magnetic anisotropy seen during SMR measurements. Finally, 2 nm of AlO$_x$ was deposited as a capping layer in order to prevent oxidation of the Co layer for all samples.

Hall bars were patterned using photolithography and Ar-ion milling with repeated parallel Hall bars (aligned either to the [001] or [1$\bar{1}$0] directions) across the entire film that have lengths of 25 μm and widths of 10 μm. A diagram of the Hall bar structure used with the definition of axes and angles used in this work can be seen in Fig. 1(a). Both flat reference samples and Pt thickness-gradient wedge samples were grown. Flat reference samples were used to calibrate the wedge sample data points to the proper thicknesses.

In this work, $\hat{x}$ is defined by the applied current direction (which depends on the Hall bar orientation relative to the crystal structure of the sample), $\hat{z}$ is defined by the out-of-plane direction, θ is the angle from the z axis, and ϕ is the angle from the x axis. Thus, it is important to note that the x and y axes are rotated depending on the orientation of the Hall bar.

X-ray reflectivity (XRR) and atomic force microscopy (AFM) were used in order to measure the roughnesses of the interfaces and surfaces, respectively, of various samples. The graphs and fits for single layer Pt(3), thin Pt(3)/Co(1) bilayer, and thick Pt(10)/Co(6) bilayer can be seen in Fig. 2(a), and the extracted roughness values in Table I. Note all samples also include an AlO$_x$ cap layer of 2 nm.
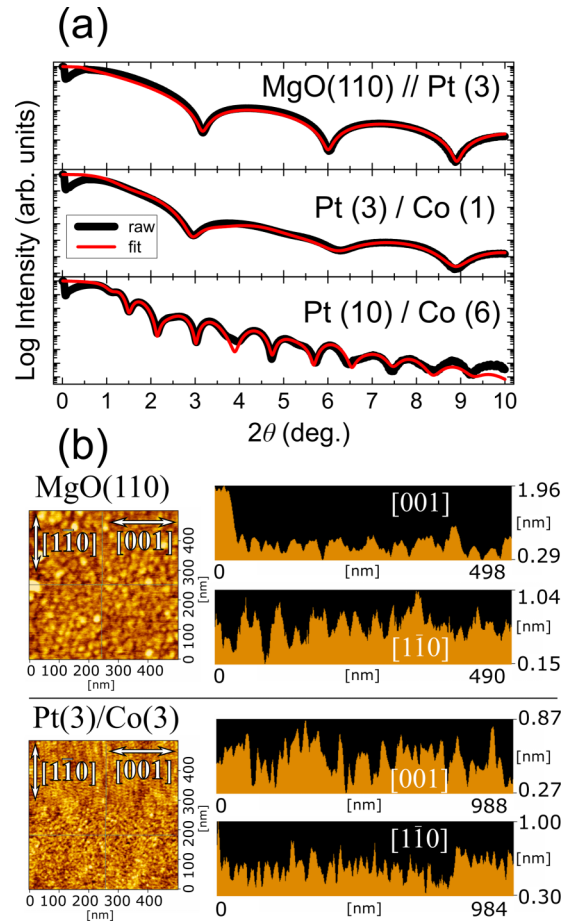

FIG. 2. (a) X-ray reflectivity measurements and fits for MgO(110)//Pt(3) (top), MgO(110)//Pt(3)/Co(1) (middle), and MgO(110)//Pt(10)/Co(6) (bottom). Results of fit can be found in Table I. (b) AFM micrographs of MgO(110) bare substrate (top) and MgO(110)//Pt(3)/Co(3)/AlO$_x$ (bottom) with corresponding line scans in both [001] and [1$\bar{1}$0] directions. White arrows describe line scan direction shown on the right.

Both the single layer Pt(3) and thin Pt(3)/Co(1) show near-perfect fitting, and the extracted roughness values are very low, less than 0.1 nm in the case of single layer Pt, and 0.1–0.2 nm for the thin bilayer case. The thicker bilayer case yielded slightly rougher values, 0.3–0.4 nm, although it can be seen the fitting is not quite as good, especially above a 2θ of $\sim 8°$. One reason for this could be a change in density from the substrate side to the cap side of the layers due to epitaxy, and more room for lattice relaxation than the thin bilayer case, making fitting slightly more difficult.

TABLE I. Roughness values of substrate/Pt and Pt/Co interfaces extracted from XRR fits seen in Fig. 2(a). Note: All samples are capped with 2 nm of AlO$_x$.

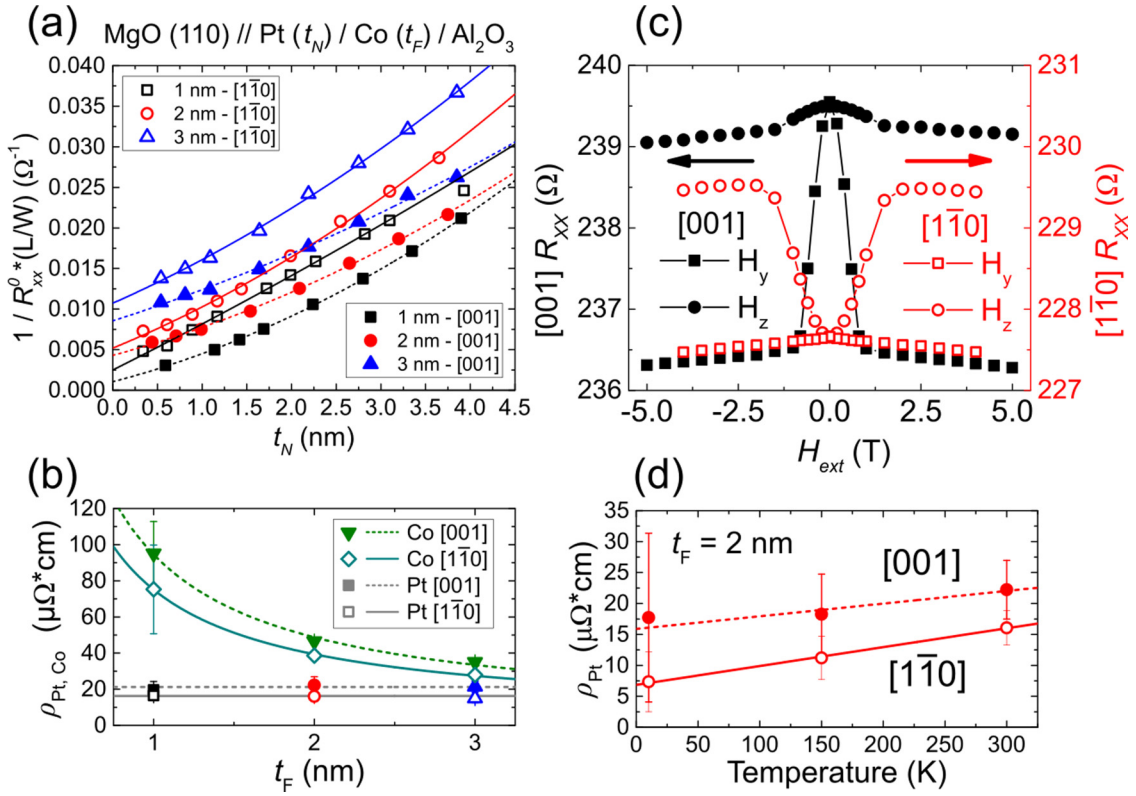| Sample structure	Substrate/Pt (nm)	Pt/Co (nm)
MgO(110)//Pt(3)	0.07	
MgO(110)//Pt(3)/Co(1)	0.10	0.23
MgO(110)//Pt(10)/Co(6)	0.39	0.27

FIG. 3. (a) Quadratic fits of sheet conductivity as a function of Pt thickness measured on Pt-wedge samples for various Co thicknesses. Legend represents points in (a), (b), and (d). (b) Calculated average resistivities of Pt and Co obtained from fits in (a) for [001] and [1$\bar{1}$0] directions (relative to Pt for Co). (c) Example of raw H_y and H_z field scans for both [001] and [1$\bar{1}$0] current directions, showing opposite behavior due to magnetocrystalline anisotropy in the Co layer. (d) Pt resistivity as a function of temperature for the 2 nm Co [001] and [1$\bar{1}$0] samples.

Qualitatively, the slope of the XRR signal is proportional to the roughness, and it can be seen the raw data has a lesser slope than the fit, indicating the calculated roughness values are slightly too high, and are likely more in line with the single layer and thin bilayer cases.

AFM was performed on a bare MgO(110) substrate and an MgO(110)//Pt(3)/Co(3)/AlO$_x$ bilayer sample. Micrographs and line scans can be seen in Fig. 2(b). Line scans were performed along the two primary in-plane directions, the [001] and [1$\bar{1}$0] directions, to confirm there is no significant discrepancy in the roughness that could be the source of the anisotropy.

Over the entire scan range, the bare MgO (110) substrate was measured to have a mean height R_a of 1.6 Å and a root mean square deviation rms of 2.1 Å. Along the [001] line scan, a R_a of 1.3 Å was found, and along the [1$\bar{1}$0] line scan, a R_a of 1.1 Å was found. These results are consistent with the specifications of the substrate supplier.

For the Pt(3)/Co(3) bilayer case, the surface was found to be even less rough. Over the entire scan range, a R_a of 0.9 Å and a rms of 1.1 Å were measured. Along the [001] line scan, a R_a of 0.8 Å was found, and along the [1$\bar{1}$0] line scan, a R_a of 0.7 Å was found.

These XRR and AFM results confirm that the bilayers are deposited very evenly with a very low roughness, and there is no significant difference in roughness between the two in-plane directions that could be a source of anisotropy.

For the fitting of the Pt thickness-dependent data, it is important to know the resistivities of both the Pt and Co layers individually, both as fitting parameters and to calculate the current shunting coefficient. Inverse sheet resistance (sheet conductance) normalized by Hall bar length L and width W ($\frac{1}{R_{xx}^0} * \frac{L}{W}$) for the bilayer system at zero applied field as a function of Pt thickness can be seen in Fig. 3(a). A quadratic fit (according to the Fuchs-Sondheimer model, see the Supplemental Material of Ref. [23] for details) is used to calculate the Pt and Co resistivities. Although the Pt resistivity is thickness dependent, the average resistivity value for the measured thickness range is used, as it makes fitting easier and has a negligible impact on fitted values.

The calculated average Pt resistivities can be seen in Fig 3(b). In the [001] direction, the Pt resistivity was found to be $\rho_{xx}^{Pt[001]} = 21.1 \pm 2.4 \ \mu\Omega\,cm$, while the [1$\bar{1}$0] direction was found to have a resistivity of $\rho_{xx}^{Pt[1\bar{1}0]} = 15.8 \pm 1.3 \ \mu\Omega\,cm$. As expected, there is no Co thickness dependence for the Pt resistivity.

Co resistivity is calculated by extrapolating to zero Pt thickness at the intercept, with the [001] direction (relative to Pt) having a slightly higher resistivity than the [1$\bar{1}$0] direction. This is likely in part due to anisotropic magnetoresistance
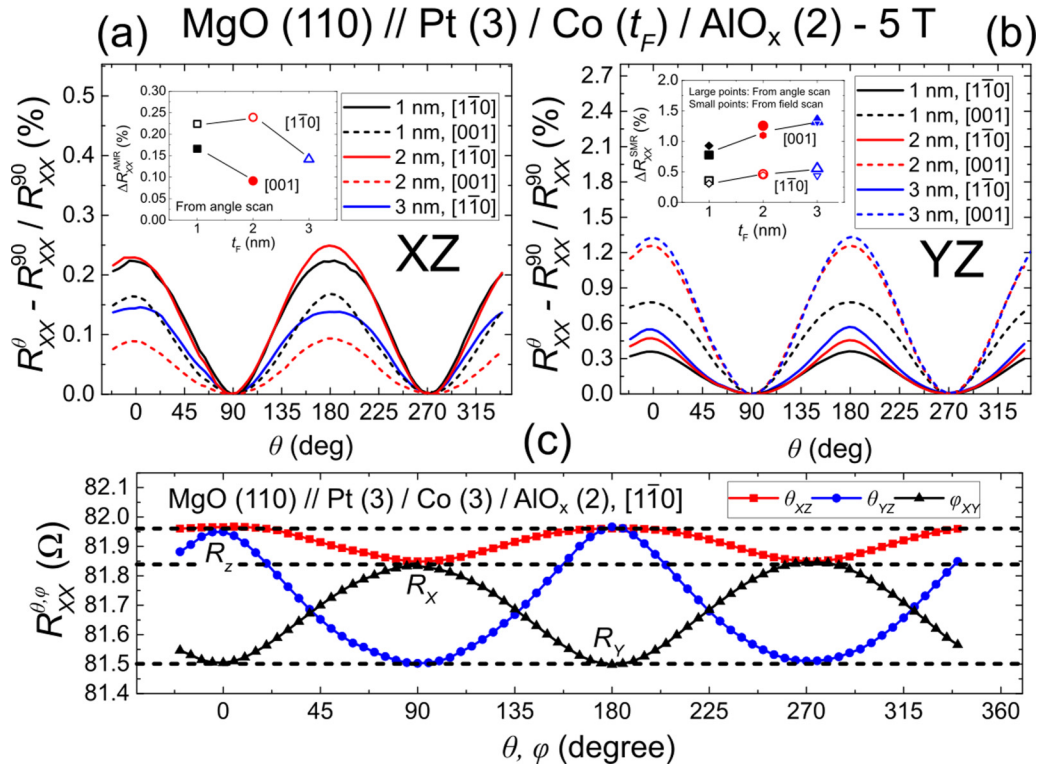
FIG. 4. (a) Field angle (θ) scans in the XZ plane for Pt(3)/Co(t_F) samples showing percent change in resistance due to AMR. Inset shows ΔR_{xx}^{AMR} extracted from angle scans. (b) Angle scans in the YZ plane for Pt(3)/Co(t_F) samples showing percent change in resistance due to SMR. Inset shows ΔR_{xx}^{SMR} extracted from angle scans. (c) Representative θ_{XZ}, θ_{YZ}, and ϕ_{XY} scans for Pt(3)/Co(3) sample aligned in the [1$\bar{1}$0] direction.

(AMR) in the Co. Because the Co layer has very strong magnetocrystalline anisotropy, the magnetization lies along [001] at zero field regardless of Hall bar orientation. Along with AMR, from measurements on MgO(110)//Co(2, 3 nm) epitaxial single layers, there also appears to be a crystallographic orientation dependence on the resistivity as well, similar to the Pt. The Co resistivity is also found to be thickness dependent, and follows the form $\rho_{Co} \propto \frac{1}{t_F}$. Since the Co layer is flat, the individual values for each thickness are used in the analysis.

Finally, it is worth noting that although there is large error in the calculation of the Co resistivity at 1 nm, this does not affect the fitting much, as it is only used in the current shunting coefficient, and even a factor of 2 difference in the Co resistivity value has negligible effects on the fitted parameters.

Since SMR measurements were also performed at 10 and 150 K on the 2 nm Co samples, Pt resistivity as a function of temperature was also measured, and can be seen in Fig. 3(d). As expected for a metal, the resistivity decreases as the temperature decreases, at approximately the same rate for both directions. From this, it can also be seen that the anisotropy in resistivity increases as temperature decreases, with the averaged $\rho_{Pt}^{[001]}$ being 38% larger than $\rho_{Pt}^{[1\bar{1}0]}$ at 300 K, 63% larger at 150 K, and 140% larger at 10 K.

In this paper, ΔR_{xx}^{SMR} is defined as the difference between longitudinal resistance when the magnetization is saturated in the $\hat{y}$ direction and when saturated in $\hat{z}$, or in other words, $\Delta R_{xx}^{SMR} = R_{xx}(H_y) - R_{xx}(H_z)$ although other magnetoresistance (MR) effects may be present [23]. In Fig. 3(c), example

field scans can be seen for Hall bars oriented in the [001] and [1$\bar{1}$0] directions, and it can be seen there is a clear difference in the behavior between the two. For [001] oriented Hall bars, there is only a small change in $R_{xx}(H_z)$, while there is a large change in $R_{xx}(H_y)$. For [1$\bar{1}$0] oriented Hall bars, this behavior is opposite.

This behavior can be explained by understanding the mechanism of SMR. In the SMR effect, a portion of the spin current generated in the Pt layer from the spin Hall effect gets reflected back into the Pt at the Pt-Co interface. This reflected spin current generates extra charge current through the inverse spin Hall effect, leading to a measurable decrease in resistance. Spin absorption into the Co layer is maximized when M is perpendicular to the spin polarization σ, which is in the $\hat{y}$ direction, and minimized when M is parallel to σ [24]. In other words, lower resistance is expected when M is in the $\hat{y}$ direction, and higher resistance when M is in the $\hat{x}$ or $\hat{z}$ direction (excluding other MR effects). Thus, the difference in behavior Fig. 3(c) can be understood from the fact that the magnetic easy axis is along the Pt [001] direction (the Co c axis), which is $\hat{x}$ for [001] and $\hat{y}$ for [1$\bar{1}$0].

III. FIELD ANGULAR DEPENDENCE

In order to measure the inherent anisotropic magnetoresistance (AMR) in the Co layer to compare to the SMR, angular dependent measurements were performed on for MgO(110)//Pt(3)/Co(1, 2, 3). AMR has a different angular
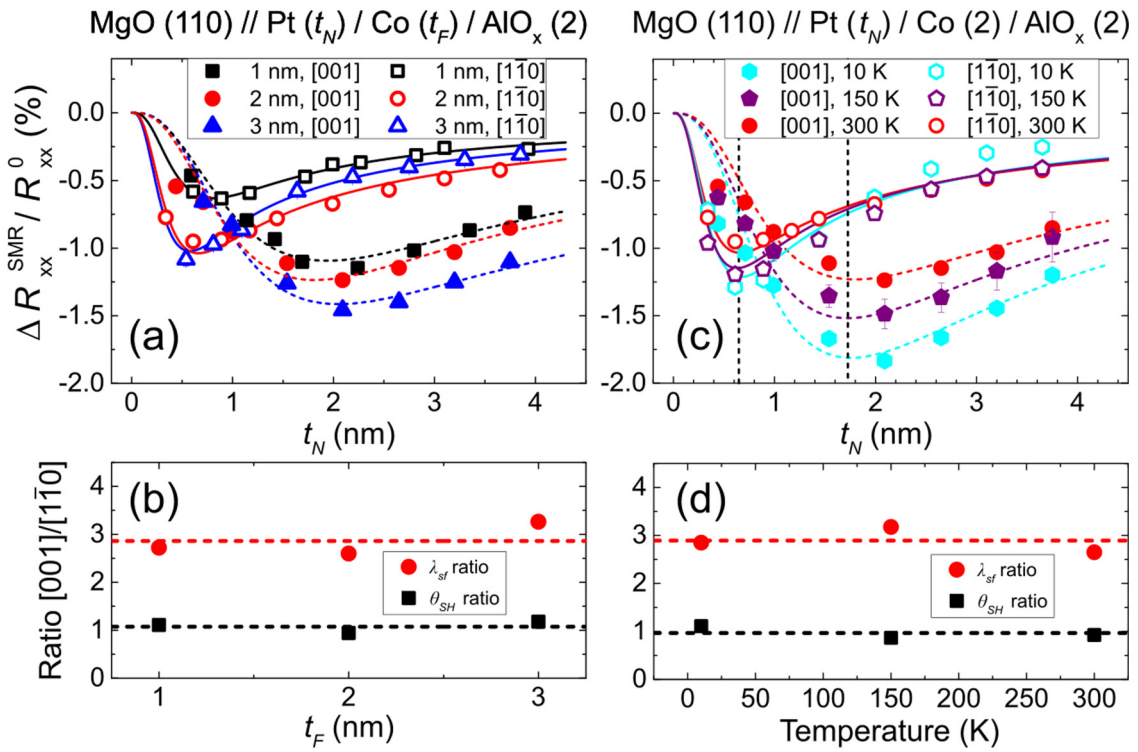
FIG. 5. (a) Pt thickness-dependent SMR for the [1$\bar{1}$0] (open points) and [001] (solid points) directions for t_F = 1, 2, 3 nm at 300 K. Solid (dashed) lines are fitted curves using Eq. (1). (b) Pt thickness-dependent SMR for the [1$\bar{1}$0] (open points) and [001] (solid points) directions 2 nm Co at T = 10, 150, and 300 K. Solid (dashed) lines are fitted curves using Eq. (1). (c) $\lambda_{sf}^{[001]}/\lambda_{sf}^{[1\bar{1}0]}$ and $\theta_{SH}^{[001]}/\theta_{SH}^{[1\bar{1}0]}$ ratios as a function of Co thickness using fit values obtained in (a). (d) $\lambda_{sf}^{[001]}/\lambda_{sf}^{[1\bar{1}0]}$ and $\theta_{SH}^{[001]}/\theta_{SH}^{[1\bar{1}0]}$ ratios as a function of temperature for 2 nm Co using fit values obtained in (b).

dependence than SMR allowing the two to be separated; AMR depends on the angle between applied current I and magnetization M, while SMR depends on the angle between spin polarization σ and magnetization M.

In the coordinates explained in Fig. 1(a), $\hat{x}$ is defined as the direction of applied I, meaning σ will be in $\hat{y}$ due to the spin Hall effect (SHE). Thus, by performing an angle scan in the XZ plane, $\Delta AMR = [R_{xx}(H_x) - R_{xx}(H_z)]/R_{xx}^0$ can be extracted, while an angle scan in the YZ plane, $\Delta SMR = [R_{xx}(H_y) - R_{xx}(H_z)]/R_{xx}^0$ is extracted. This measurement is performed at 5 T to fully saturate magnetization in the direction of the applied field, and in the case of the YZ scan, should be equivalent to the values extracted using field scans as shown in Fig. 5(a) at t_N = 3 nm.

Figure 4(a) shows the results of the XZ angle scans, while its inset shows the extracted ΔAMR values. For all thicknesses, [1$\bar{1}$0] shows a larger AMR signal than for [001], while the overall trend for both directions is decreasing AMR with increasing Co thickness. It has been shown previously that the AMR depends on the direction of applied current in epitaxial Fe films, and that the trend of increasing or decreasing AMR with thickness also depends on current direction [25].

Figure 4(b) shows the results of the YZ angle scans, with the inset showing the extracted ΔSMR values, along with the values from the field scans done in the Pt thickness dependence section. As expected, the values all match between the angle and field scans. The [001] direction shows a larger

SMR signal for all Co thickness than the [1$\bar{1}$0] direction, and the overall trend for both is an increasing SMR signal with increasing Co thickness.

If we compare the magnitudes of the MR signals, we can see that the AMR signal is much smaller than the SMR signal for both directions and all thicknesses; at most it is 50% of the SMR signal for 1 and 2 nm [1$\bar{1}$0] Co, while it is much smaller for [001], less than 10% the magnitude for 2 nm [001] Co. Next, surprisingly, not only is the overall trend with Co thickness opposite for AMR and SMR measurements, but also the current direction with the larger signal is opposite.

It has also recently been suggested that the crystalline structure of the FM layer can influence the MR in the YZ plane, in other words influencing the SMR signal. Isogami *et al.* [26] showed that in the indium tungsten oxide (IWO) bilayers IWO/Co and IWO/CoFe, MR in the YZ plane of around 0.2% was seen that was not due to SMR. This MR only appeared when the Co and CoFe layers formed grains with a preferred crystal orientation, but disappeared when the FM layer was disordered. MR in the YZ plane was investigated on single layer MgO(110)//Co(2, 3 nm) samples, but only signals between 0.01%–0.1% were observed (depending on current direction), meaning this cannot explain the large anisotropy seen in this work.

One final point to take into account is the relation of resistance when magnetization is perpendicular to the plane

$(\hat{z}, R_p)$, when magnetization is parallel to applied current $(\hat{x}, R_\parallel)$, and when magnetization is transverse to applied current $(\hat{y}, R_\perp)$. The relative resistances depend on how the various MR contributions interact and combine. In most cases, $R_\parallel$ is greater than or equal to R_p and $R_\perp$, due to the main contributions of the AMR and SMR effects, along with other contributions such as the geometrical size effect (GSE) or interfacial effects [27]. In this work, however, the relation was found to be $R_p > R_\parallel > R_\perp$. This unusual relation arises due to a combination of the standard negative SMR signal and the nonstandard negative AMR signal. This relation was previously observed in epitaxial Co/Pt grown on MgO(111), and was attributed to a negative GSE that leads to R_p being greater than R_{ip} (in-plane resistance) [28].

IV. Pt THICKNESS AND TEMPERATURE DEPENDENCE

SMR as a function of Pt layer thickness (t_N) has been measured at 300 K for MgO(110)//Pt(t_N)/Co(1, 2, 3) bilayer systems in order to extract spin Hall angle (θ_{SH}) and spin diffusion length (λ_{sf}) through fitting using the following equation [23]:

$$\frac{\Delta R_{xx}^{SMR}}{R_{xx}^0} = -\theta_{SH}^2 \frac{\lambda_{sf}}{t_N} \frac{\tanh(\tau)}{1+\eta}\left[1 - \frac{1}{\cosh(2\tau)}\right], \quad (1)$$

where $\eta = (\rho_N t_F)/(\rho_F t_N)$ is the current shunting coefficient and $\tau = \frac{t_N}{2\lambda_{sf}}$. In this form of the drift-diffusion model of SMR for a HM/FM bilayer, a transparent Pt/Co interface is assumed, and longitudinal spin absorption into the Co layer is neglected [29]. This fitting gives a lower bound on the spin Hall angle [23]. The results of this fitting can be seen in Fig. 5(a).

Good fitting is obtained for Hall bar devices aligned along both primary directions, although the signal for each direction is strikingly different. When current is applied along the [1$\bar{1}$0] direction, the SMR signal reaches a maximum around 1 nm thick Pt, while for the [001] direction the signal does not reach a maximum until around 2 nm of Pt. Above 2 nm of Pt, the [001] direction shows a signal more than 2× larger than [1$\bar{1}$0]. The fitting at very low thicknesses, especially for the [001] direction, deviates from the raw data, however. The YZ MR in this thinner region is likely affected by bulk-interface charge-spin entanglement [3]. However, the data that are well fit at thicker regions should be dominated by bulk effects, which approximately determine the spin diffusion length. A summary of extracted parameters can be seen in Table II.

As expected, the spin diffusion length is roughly independent of the Co layer thickness, while the spin Hall angle increases with increasing Co thickness. Although one might expect the spin Hall angle to decrease as the FM layer thickness increases due to extra current shunting into the FM layer, it has been shown that for Pt/Co layers, the spin Hall angle increases at least up to at 7 nm Co. The extracted spin Hall angles are also consistent with this previous report [23].

While there may be a small enhancement of the spin Hall angle for Hall bars aligned along the [001] direction, the primary reason for the large discrepancy between the two current directions. According to the fitting results, the spin diffusion length for the [001] direction is ~0.6–0.75 nm, and is extremely short in the [1$\bar{1}$0] direction at ~0.20–0.26 nm.

TABLE II. Extracted θ_{SH} and λ_{sf} values from fits of data shown in Figs. 5(a) and 5(b) using Eq. (1).

t_F, orientation	θ_{SH}	λ_{sf} (nm)
1 nm, [1$\bar{1}$0]	0.20 ± 0.003	0.26 ± 0.01
2 nm, [1$\bar{1}$0]	0.29 ± 0.004	0.23 ± 0.01
3 nm, [1$\bar{1}$0]	0.27 ± 0.01	0.20 ± 0.02
1 nm, [001]	0.21 ± 0.003	0.75 ± 0.04
2 nm, [001]	0.26 ± 0.004	0.61 ± 0.03
3 nm, [001]	0.33 ± 0.005	0.62 ± 0.03
Temp., orientation	θ_{SH}	λ_{sf} (nm)
10 K, [1$\bar{1}$0]	0.26 ± 0.009	0.23 ± 0.02
150 K, [1$\bar{1}$0]	0.32 ± 0.005	0.18 ± 0.01
300 K, [1$\bar{1}$0]	0.31 ± 0.006	0.19 ± 0.01
10 K, [001]	0.29 ± 0.004	0.65 ± 0.03
150 K, [001]	0.28 ± 0.005	0.58 ± 0.03
300 K, [001]	0.26 ± 0.004	0.61 ± 0.03

This is much shorter than the values λ_{sf} that have been reported, which generally range from 1–11 nm [30–35], but has been reported to be as small as 0.5 nm [36].

Since λ_{sf} normally depends on the resistivity, it can be useful to calculate the $\lambda_{sf}\rho_{Pt}$ product. For the [1$\bar{1}$0] direction,

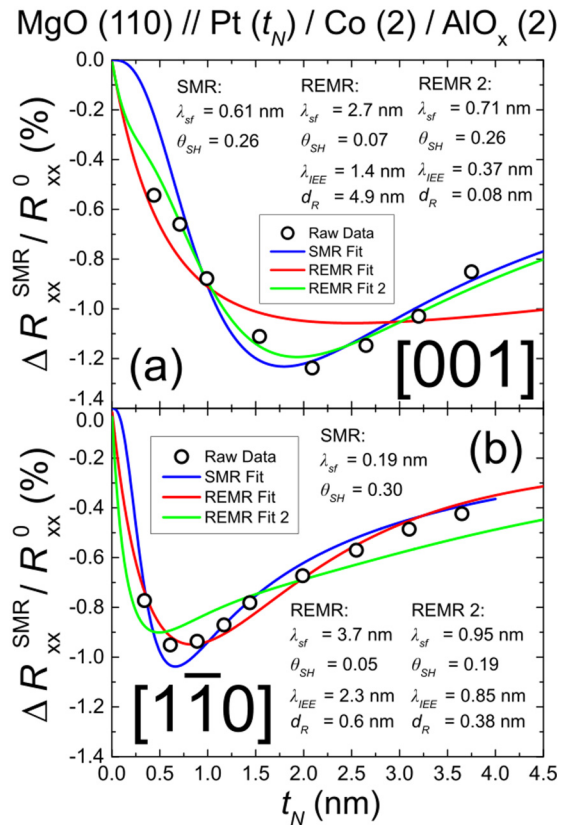FIG. 6. Comparison of fitting using the standard SMR model and the modified REMR model for Co (2 nm) samples for (a) the [001] and (b) the [1$\bar{1}$0] current directions. Note that λ_{sf} and θ_{SH} are fitting parameters for the SMR model, but are constants for the REMR model.

this product comes out to be $(0.53 \pm 0.04) \times 10^{-16} \ \Omega \, \text{m}^2$, while for the [001] direction the product is $(1.34 \pm 0.2) \times 10^{-16} \ \Omega \, \text{m}^2$. This is around one order of magnitude smaller than previously reported values by Sagasta *et al.* [14] of $(6.1 \pm 0.2) \times 10^{-16} \ \Omega \, \text{m}^2$ and Nguyen *et al.* [30] of $(7.7 \pm 0.8) \times 10^{-16} \ \Omega \, \text{m}^2$, although it is important to note that the work by Nguyen *et al.* assumed the EY mechanism, which cannot be the mechanism in this work for a number of reasons. In the EY mechanism $\lambda_{sf} \propto \rho_{\text{Pt}}^{-1}$, but in this work $\lambda_{sf}^{[1\bar{1}0]} < \lambda_{sf}^{[001]}$ and $\rho_{\text{Pt}}^{[1\bar{1}0]} < \rho_{\text{Pt}}^{[001]}$. Normally the EY mechanism is expected in metals because of their short mean free path, but these results are inconsistent with the EY mechanism. Here we note that because of this inconsistency, the values obtained and shown in Table II may not be quantitatively correct. However, the spin diffusion length must be anisotropic in order to explain the difference in shape and peak position seen in Figs. 5(a) and 5(c).

This inconsistency with the EY mechanism is further seen by performing SMR measurements at varying temperatures. As seen in Fig. 5(b) for a 2 nm Co sample, when the temperature was lowered to 150 K and further to 10 K, there was no shift in the peak position for either current direction. In the EY mechanism, when the resistivity is lowered at lower temperatures, the spin diffusion length should increase, which causes a shift in the SMR peak position. As shown in Fig. 3(d), there is indeed a significant decrease in resistivity for both directions, but no peak shift is seen at any temperature. This has previously been used as an argument for the dominance of the DP mechanism [37], although this must be considered very carefully.

The origin of the SMR effect, and thus the basis of the diffusion model, is assumed to arise from the spin Hall effect [38,39], which is a bulk effect. The DP mechanism, on the other hand, is an interfacial effect. Although it may qualitatively explain no peak shift, simply replacing the spin diffusion length from the bulk due to the EY mechanism with the spin diffusion length due to the interfacial spin-orbit coupling may not be quantitatively correct in the fitting equation. The spin diffusion length can be calculated for a DP dominated system ($\tau_s \approx \tau_{s,\text{DP}}$) as [37,40]

$$\lambda_{sf} = \sqrt{D\tau_s} = \sqrt{\frac{D}{\langle \Omega_k^2 \rangle \tau_p}} = \sqrt{\frac{v_F^2}{\langle \Omega_k^2 \rangle}}, \tag{2}$$

where the spin relaxation time for the DP mechanism τ_s is $\frac{1}{\tau_s} = \tau_p \langle \Omega_k^2 \rangle$, with $\langle \Omega_k^2 \rangle$ being the spin precession vector proportional to the Rashba parameter α_{BR}, the momentum scattering time $\tau_p = \frac{D}{v_F^2}$, D is the diffusion constant, and $v_F = \sqrt{\frac{2E_F}{m}}$ is the Fermi velocity [41]. λ_{sf} is independent of both t_N and T, and only depends on the Fermi velocity (which should be roughly independent of T for a metal, as metals have a Fermi energy much larger than the thermal energy $k_B T$) and the Rashba parameter. The Fermi surface of Pt is known to be anisotropic, with the Fermi velocity in the [110] direction being about twice as large as in the [001] direction [42], but this alone cannot explain the $\lambda_{sf}^{[001]}/\lambda_{sf}^{[1\bar{1}0]}$ ratio of 3 as seen in Figs. 5(c) and 5(d). As such, this result implies there is anisotropy in the spin precession vector, and therefore anisotropy in the Rashba parameter.

Although there is large anisotropy in the spin diffusion length, the spin Hall angle obtained from the fitting is approximately isotropic. It is difficult to say whether or not this is to be expected. In general, the spin Hall effect is expected to be isotropic for cubic systems from first principles [43], and epitaxial MgO(100)//Fe/Pt was recently reported to have an isotropic spin Hall angle [44]. On the other hand, the RE effect can give rise to Rashba-Edelstein magnetoresistance (REMR), which was found in Bi/Ag/CoFeB trilayers to have the same angular dependence as SMR [10]. However, the MR in this report that is due to the REMR is more than one order of magnitude smaller than the SMR in the current work.

V. REMR MODEL FITTING

An expanded SMR model that includes the REMR has been recently developed, which incorporates $e(\lambda_{\text{IEE}}\hat{z} \times \boldsymbol{E})$ spin accumulation contributions from the RE effect into the SMR theory. This hybrid MR is calculated using the following equation [45]:

$$\frac{\Delta R_{xx}}{R_0} \approx -\frac{\lambda_{sf}/\rho_N}{t_N/\rho_N + t_F/\rho_F} \text{Re}\left[\frac{2\rho_N \lambda_{sf} G_{\uparrow\downarrow}}{1 + 2\rho_N \lambda_{sf} G_{\uparrow\downarrow} \coth(t_N/\lambda_{sf})}\right]\left\{\left[\theta_{\text{SH}} \tanh\left(\frac{t_N}{2\lambda_{sf}}\right) + \left(\frac{\lambda_{\text{IEE}}}{2\lambda_{sf}}\right)\right]^2\right.$$

$$\left. - 2\left(\frac{\lambda_{\text{IEE}}}{2\lambda_{sf}}\right)\left[\theta_{\text{SH}} \tanh\left(\frac{t_N}{2\lambda_{sf}}\right) + \left(\frac{\lambda_{\text{IEE}}}{2\lambda_{sf}}\right)\right]\frac{\langle \sinh[(t_N - d_2)/\lambda_{sf}] \rangle}{\sinh(t_N/\lambda_{sf})} + \left(\frac{\lambda_{\text{IEE}}}{2\lambda_{sf}}\right)^2 \frac{\langle \sinh^2[(t_N - d_2)/\lambda_{sf}] \rangle}{\sinh^2(t_N/\lambda_{sf})}\right\}. \tag{3}$$

Here λ_{IEE} is the inverse Edelstein length, a unit with dimensions of length that corresponds to the electron's spin-momentum locking distance [46,47], d_2 is the thickness of the RE region, $G_{\uparrow\downarrow}$ is the spin-mixing conductance at the HM/FM interface, and $\langle \cdots \rangle$ is the average with respect to d_2 weighted by $\exp(-d_2/d_R)$, where d_r is the effective thickness of the RE region (see the Supplemental Material of Ref. [45] for more details).

In this model, the EY spin relaxation mechanism and the intrinsic/side-jump contributions are assumed to dominate the bulk of the epitaxial Pt, so λ_{sf} and θ_{SH} are first precalculated based on the Pt resistivity and the $\lambda_{sf}\rho_{\text{Pt}}$ and $\lambda_{sf}\theta_{\text{SH}}$ products. The $\lambda_{sf}\rho_{\text{Pt}}$ product has been suggested to be $\sim 0.6 \times 10^{-15} \ \Omega \, \text{m}^2$ by theory [48] and experiment [14], so this value is used with the calculated ρ_{Pt} values to calculate $\lambda_{sf}^{[001]} = 2.7$ nm and $\lambda_{sf}^{[1\bar{1}0]} = 3.7$ nm. The $\lambda_{sf}\theta_{\text{SH}}$ product is set to 0.2 nm [32,49], resulting in $\theta_{\text{SH}}^{[001]} = 0.07$ and $\theta_{\text{SH}}^{[1\bar{1}0]} = 0.05$. The real part of $G_{\uparrow\downarrow}$ is assumed to be $10^{15} \ \Omega^{-1} \, \text{m}^{-2}$ [50].

Using these values, the data for the $t_F = 2$ nm samples were fit using this model to yield the red curves seen in Fig. 6, with d_R and λ_{IEE} as fitting parameters. For the [$1\bar{1}0$] direction

[Fig. 6(b)], the fit seems reasonable and gives similar values to the work in Ref. [45]. However, the fit is very poor for the [001] direction using the values calculated assuming the bulk EY contribution. In order to create a good fit, $\lambda_{sf}^{[001]}$ must be decreased to 0.71 nm and $\theta_{SH}^{[001]}$ must be increased to 0.26, as shown by the green curve in Fig. 6(a) (labeled REMR Fit 2).

However, if we take these parameters to be the "true" values, and calculate $\lambda_{sf}^{[1\bar{1}0]}$ and $\theta_{SH}^{[1\bar{1}0]}$ assuming a constant $\lambda_{sf}\rho_{Pt}$ and $\lambda_{sf}\theta_{SH}$ from the EY mechanism, we obtain the result shown by the green curve in Fig. 6(b), which can be seen to be a poor fit. From this, we can conclude that the assumption of the bulk EY contribution due to the Pt resistivity is not valid for this system.

VI. CONCLUSION

It has been demonstrated that epitaxial Pt/Co bilayers on MgO(110) show strongly anisotropic spin Hall magnetoresistance, with [001]-oriented devices having an SMR magnitude magnitude over 2× greater than [1$\bar{1}$0] devices at Pt thicknesses above 2 nm. SMR results at various temperatures and the directly proportional relationship between λ_{sf} and ρ_{Pt} for the two directions implies that the DP spin relaxation mechanism is dominant. From the definition of λ_{sf} in a DP dominated system, it is suggested that anisotropy in both the Fermi surface and RE effect give rise to this anisotropic λ_{sf}. While there is still work to be done in developing new theory that can accurately model epitaxial systems such as this one, this work helps pave the way for a deeper understanding of anisotropic spin transport in epitaxial HM/FM systems.

[1] A. Manchon, J. Železný, I. M. Miron, T. Jungwirth, J. Sinova, A. Thiaville, K. Garello, and P. Gambardella, Rev. Mod. Phys. **91**, 035004 (2019).

[2] J. Sinova, S. O. Valenzuela, J. Wunderlich, C. H. Back, and T. Jungwirth, Rev. Mod. Phys. **87**, 1213 (2015).

[3] Y. Du, H. Gamou, S. Takahashi, S. Karube, M. Kohda, and J. Nitta, Phys. Rev. Appl. **13**, 054014 (2020).

[4] E. Rashba, Sov. Phys. Solid State **2**, 1109 (1960).

[5] E. I. Rashba and Y. A. Bychkov, J. Phys. C **17**, 6039 (1984).

[6] V. M. Edelstein, Solid State Commun. **73**, 233 (1990).

[7] H. Gamou, Y. Du, M. Kohda, and J. Nitta, Phys. Rev. B **99**, 184408 (2019).

[8] H. Li, G. Wang, D. Li, P. Hu, W. Zhou, X. Ma, S. Dang, S. Kang, T. Dai, F. Yu, X. Zhou, S. Wu, and S. Li, Appl. Phys. Lett. **114**, 092402 (2019).

[9] A. Manchon, H. C. Koo, J. Nitta, S. M. Frolov, and R. A. Duine, Nat. Mater. **14**, 871 (2015).

[10] H. Nakayama, Y. Kanno, H. An, T. Tashiro, S. Haku, A. Nomura, and K. Ando, Phys. Rev. Lett. **117**, 116602 (2016).

[11] C. Ortiz Pauyac, X. Wang, M. Chshiev, and A. Manchon, Appl. Phys. Lett. **102**, 14 (2013).

[12] I. M. Miron, G. Gaudin, S. Auffret, B. Rodmacq, A. Schuhl, S. Pizzini, J. Vogel, and P. Gambardella, Nat. Mater. **9**, 230 (2010).

[13] S. E. Barnes, J. Ieda, and S. Maekawa, Sci. Rep. **4**, 4105 (2014).

[14] E. Sagasta, Y. Omori, M. Isasa, M. Gradhand, L. E. Hueso, Y. Niimi, Y. C. Otani, and F. Casanova, Phys. Rev. B **94**, 060412(R) (2016).

[15] R. J. Elliot, Phys. Rev. **96**, 266 (1954).

[16] Y. Yafet, Phys. Rev. **85**, 478 (1952).

[17] D. Lubzens and S. Schultz, Phys. Rev. Lett. **36**, 1104 (1976).

[18] M. Johnson and R. H. Silsbee, Phys. Rev. Lett. **55**, 1790 (1985).

[19] M. Gradhand, M. Czerner, D. V. Fedorov, P. Zahn, B. Y. Yavorsky, L. Szunyogh, and I. Mertig, Phys. Rev. B **80**, 224413 (2009).

[20] M. Gradhand, D. V. Fedorov, P. Zahn, and I. Mertig, Phys. Rev. B **81**, 020403(R) (2010).

[21] M. Dyakonov and V. Perel, JETP Lett. **13**, 467 (1971).

[22] J. Ryu, M. Kohda, and J. Nitta, Phys. Rev. Lett. **116**, 256802 (2016).

[23] M. Kawaguchi, D. Towa, Y. C. Lau, S. Takahashi, and M. Hayashi, Appl. Phys. Lett. **112**, 202405 (2018).

[24] H. Nakayama, M. Althammer, Y.-T. Chen, K. Uchida, Y. Kajiwara, D. Kikuchi, T. Ohtani, S. Geprägs, M. Opel, S. Takahashi, R. Gross, G. E. W. Bauer, S. T. B. Goennenwein, and E. Saitoh, Phys. Rev. Lett. **110**, 206601 (2013).

[25] M. Tondra, D. K. Lottis, K. T. Riggs, Y. Chen, E. D. Dahlberg, and G. A. Prinz, J. Appl. Phys. **73**, 6393 (1993).

[26] S. Isogami, J. Uzuhashi, T. Ohkubo, and M. Hayashi, Phys. Rev. Mater. **3**, 024408 (2019).

[27] L. K. Zou, Y. Zhang, L. Gu, J. W. Cai, and L. Sun, Phys. Rev. B **93**, 075309 (2016).

[28] X. Xiao, J. X. Li, Z. Ding, J. H. Liang, L. Sun, and Y. Z. Wu, Appl. Phys. Lett. **108**, 222402 (2016).

[29] J. Kim, P. Sheng, S. Takahashi, S. Mitani, and M. Hayashi, Phys. Rev. Lett. **116**, 097201 (2016).

[30] M. H. Nguyen, D. C. Ralph, and R. A. Buhrman, Phys. Rev. Lett. **116**, 126601 (2016).

[31] Z. Feng, J. Hu, L. Sun, B. You, D. Wu, J. Du, W. Zhang, A. Hu, Y. Yang, D. M. Tang, B. S. Zhang, and H. F. Ding, Phys. Rev. B **85**, 214423 (2012).

[32] J. C. Rojas-Sánchez, N. Reyren, P. Laczkowski, W. Savero, J. P. Attané, C. Deranlot, M. Jamet, J. M. George, L. Vila, and H. Jaffrès, Phys. Rev. Lett. **112**, 106602 (2014).

[33] L. Liu, R. A. Buhrman, and D. C. Ralph, arXiv:1111.3702v3.

[34] M. Morota, Y. Niimi, K. Ohnishi, D. H. Wei, T. Tanaka, H. Kontani, T. Kimura, and Y. Otani, Phys. Rev. B **83**, 174405 (2011).

[35] K. Kondou, S. Mitani, S. Kasai, H. Sukegawa, and K. Tsukagoshi, Appl. Phys. Express **5**, 073002 (2012).

[36] C. T. Boone, H. T. Nembach, J. M. Shaw, and T. J. Silva, J. Appl. Phys. **113**, 153906 (2013).

[37] L. Ma, L. Lang, J. Kim, Z. Yuan, R. Wu, S. Zhou, and X. Qiu, Phys. Rev. B **98**, 224424 (2018).

[38] M. Althammer, S. Meyer, H. Nakayama, M. Schreier, S. Altmannshofer, M. Weiler, H. Huebl, S. Geprägs, M. Opel, R. Gross, D. Meier, C. Klewe, T. Kuschel, J.-M. Schmalhorst, G. Reiss, L. Shen, A. Gupta, Y.-T. Chen, G. E. W. Bauer, E. Saitoh, and S. T. B. Goennenwein, Phys. Rev. B **87**, 224401 (2013).

[39] Y.-T. Chen, S. Takahashi, H. Nakayama, M. Althammer, S. T. B. Goennenwein, E. Saitoh, and G. E. W. Bauer, Phys. Rev. B **87**, 144411 (2013).

[40] T. Valet and A. Fert, Phys. Rev. B **48**, 7099 (1993).

[41] I. Žutić, J. Fabian, and S. Das Sarma, Rev. Mod. Phys. **76**, 323 (2004).

[42] D. H. Dye, J. B. Ketterson, and G. W. Crabtree, J. Low Temp. Phys. **30**, 813 (1978).

[43] F. Freimuth, S. Blügel, and Y. Mokrousov, Phys. Rev. Lett. **105**, 246602 (2010).

[44] C. Guillemard, S. Petit-Watelot, S. Andrieu, and J.-C. Rojas-Sánchez, Appl. Phys. Lett. **113**, 262404 (2018).

[45] Y. Du, S. Karube, H. Gamou, J. Ryu, S. Takahashi, M. Kohda, and J. Nitta, arXiv:1807.10867.

[46] J. C. Sánchez, L. Vila, G. Desfonds, S. Gambarelli, J. P. Attané, J. M. De Teresa, C. Magén, and A. Fert, Nat. Commun. **4**, 2944 (2013).

[47] E. Lesne, Y. Fu, S. Oyarzun, J. C. Rojas-Sánchez, D. C. Vaz, H. Naganuma, G. Sicoli, J. P. Attané, M. Jamet, E. Jacquet, J. M. George, A. Barthélémy, H. Jaffrès, A. Fert, M. Bibes, and L. Vila, Nat. Mater. **15**, 1261 (2016).

[48] Y. Liu, Z. Yuan, R. J. H. Wesselink, A. A. Starikov, M. van Schilfgaarde, and P. J. Kelly, Phys. Rev. B **91**, 220405(R) (2015).

[49] L. Wang, R. J. H. Wesselink, Y. Liu, Z. Yuan, K. Xia, and P. J. Kelly, Phys. Rev. Lett. **116**, 196602 (2016).

[50] C. F. Pai, Y. Ou, L. H. Vilela-Leão, D. C. Ralph, and R. A. Buhrman, Phys. Rev. B **92**, 064426 (2015).